

See discussions, stats, and author profiles for this publication at: <https://www.researchgate.net/publication/3332598>

# Modeling and Identification for High-Performance Robot Control: An RRR-Robotic Arm Case Study

**Article** in IEEE Transactions on Control Systems Technology · December 2004

DOI: 10.1109/TCST.2004.833641 · Source: IEEE Xplore

---

CITATIONS

99

---

READS

6,139

4 authors, including:



[Dragan Kostic](#)

ASMPT

65 PUBLICATIONS 855 CITATIONS

[SEE PROFILE](#)



[M. Steinbuch](#)

Eindhoven University of Technology

634 PUBLICATIONS 12,222 CITATIONS

[SEE PROFILE](#)

# Modeling and Identification for High-Performance Robot Control: An RRR-Robotic Arm Case Study

Dragan Kostić, *Student Member, IEEE*, Bram de Jager, Maarten Steinbuch, *Senior Member, IEEE*, and Ron Hensen

**Abstract**—This paper explains a procedure for getting models of robot kinematics and dynamics that are appropriate for robot control design. The procedure consists of the following steps: 1) derivation of robot kinematic and dynamic models and establishing correctness of their structures; 2) experimental estimation of the model parameters; 3) model validation; and 4) identification of the remaining robot dynamics, not covered with the derived model. We give particular attention to the design of identification experiments and to online reconstruction of state coordinates, as these strongly influence the quality of the estimation process. The importance of correct friction modeling and the estimation of friction parameters are illuminated. The models of robot kinematics and dynamics can be used in model-based nonlinear control. The remaining dynamics cannot be ignored if high-performance robot operation with adequate robustness is required. The complete procedure is demonstrated for a direct-drive robotic arm with three rotational joints.

**Index Terms**—Friction, identification, Kalman filtering, modeling, robot dynamics, robot kinematics, robots.

## I. INTRODUCTION

THERE is a lasting challenge to increase the speed of robot motions, while preserving a prescribed accuracy of robot-tip positioning and/or trajectory tracking. As the performance of industrial robots is improved, robustness against uncertainty in the robot dynamics and against disturbances must be maintained. To achieve faster and more accurate robot motions, we need relevant models of both kinematics and dynamics. A kinematic model provides a relation between joint configuration and robot-tip position and orientation. It also reveals singular robot configurations that must be avoided. A dynamic model determines the control inputs needed to realize a reference motion. It also enables an analysis of how particular dynamic effects influence overall robot behavior.

This paper discusses all the necessary steps a control engineer must take to enable high-performance model-based control of a robot. These steps are: 1) kinematic and dynamic modeling of the robot; 2) obtaining model parameters via direct measurements and/or identification; 3) establishing the correctness of the structure of the models and validating the estimated

parameters; and 4) deducing to what extent the model covers the real robot dynamics, and, if needed for high-performance control, identification of the dynamics not covered with the derived model. Better quality resulting from each of these steps contributes to better performance of robot control.

In the paper, we suggest a procedure one may apply to successfully complete all the steps listed above. As it leads to robot models appropriate for high-performance control, the procedure looks quite appealing for use in practice. Its theoretical foundation is already well-known and is sufficiently elaborated in the literature. This is addressed in an extensive overview of available results on modeling and identification of robot kinematics, dynamics and friction effects, given in the next section. The effectiveness of the procedure we suggest in this paper is demonstrated with a case study. We model a particular class of robotic manipulators and identify one representative from this class. However, the procedure is applicable to any other class of robots, which in turn implies its general relevance.

A robotic arm with three revolute joints (RRR kinematics), implemented as waist, shoulder and elbow, is our test bed for modeling and identification. The kinematics of this arm is very common in industry: the first three degrees-of-freedom of the PUMA 560 or the KUKA IR 361 robots are implemented in this fashion. Therefore, the results presented in this paper can be directly employed in industry. To stress the influence of nonlinear dynamic couplings between the robot axes, we consider a direct-drive actuation for the robot. It is well-known that with a transmission between joint actuators and links, nonlinear couplings can become small [1]–[3]. Consequently, some dynamic effects may have a smaller contribution to the overall dynamic behavior, and, in turn, accurate knowledge of their parameters does not influence the effectiveness of the complete dynamic model in model-based control. This facilitates the estimation of model parameters and the robot control problem itself. With direct-drive actuation all couplings remain [4], [5], and accurate estimation of parameters becomes essential. As a particular representative of this robot class, we use the RRR robotic arm available at Eindhoven University of Technology, The Netherlands [6], [7]. Our objectives are as follows: modeling of the RRR-arm kinematics and rigid-body dynamics, estimation of its friction and inertial parameters, and identification of the arm dynamics not covered with the rigid-body model.

The first step is to derive both kinematic and rigid-body dynamic models in closed-form, and thus facilitate model analysis and manipulation, and the design of model-based control laws. The correct structure of both models will be established in a representative motion task. The next step is to estimate the model parameters. It is assumed that the kinematic parameters are already known with a sufficient accuracy, so emphasis will

Manuscript received January 17, 2003; revised October 24, 2003. Manuscript received in final form March 3, 2004. Recommended by Associate Editor K. Kozłowski.

D. Kostić, B. de Jager, and M. Steinbuch are with the Dynamics and Control Technology Group, Department of Mechanical Engineering, Technische Universiteit Eindhoven, 5600 MB Eindhoven, The Netherlands (e-mail: D.Kostic@tue.nl; A.G.de.Jager@wfw.wtb.tue.nl; M.Steinbuch@tue.nl).

R. Hensen is with the Technical Analysis Group, DAF Trucks N.V., Eindhoven, The Netherlands (e-mail: Ron.Hensen@DAFTRUCKS.com).

Digital Object Identifier 10.1109/TCST.2004.833641

be on estimating the friction and inertial parameters. To establish experimental conditions allowing for the simplest and the most time-efficient least-squares estimation of the inertial parameters, we will online reconstruct the robot motion coordinates using Kalman observers. The rules for observers' tuning will be particularly addressed. Guidelines for the design of joint trajectories, used in identification experiments, will be highlighted. Results of the experimental parameter estimation will be presented. The third step is experimental validation of the obtained kinematic and dynamic models. The dynamic model will be used to compensate for particular effects of the actual robot dynamics. As the final step, we will explain how to identify flexible dynamics, not covered with the rigid-body dynamic model.

The paper is organized as follows. Section II summarizes available results on robot modeling and identification. In Section III, kinematic and rigid-body dynamic models for the considered robot class are derived, and their correctness is established. Section IV is a case-study. It describes the setup used in experiments, methodology for friction modeling and estimation, calculation of trajectories used in identification experiments, online reconstruction of the motion coordinates, estimation of inertial parameters of the rigid-body dynamic model, results of experimental validation of the models, and identification of the flexible dynamics. Conclusions will come at the end.

## II. ROBOT MODELING AND IDENTIFICATION—AN OVERVIEW

### A. Modeling of Robot Kinematics and Dynamics

The robotics literature offers various tutorials on both kinematic and dynamic modeling [1]–[3], [5], [8]. A number of modeling methods are available, meeting various requirements. As for robot kinematics, the model is a mapping between the task space (in general a 6-dimensional space of robot-tip coordinates) and the joint space (dimension equal to the number of robot degrees of freedom). The mapping from the joint to the task space is called the forward kinematics. The opposite mapping is the inverse kinematics. These mappings can be represented as recursive or closed-form algebraic models. The algebraic closed-form representation facilitates manipulation of the models and enables a straightforward mathematical analysis. As high accuracy of computation can be achieved faster with the closed-form models, they are preferable for real-time control. Dynamic models relate motions, speeds and accelerations with applied control inputs (forces/torques). A variety of methods are available for their derivation, and, as with kinematic models, they can be represented in various forms. Algebraic recursive models require less computational effort and admit a very compact form of representation. These are the traditional arguments why algebraic recursions are preferable for real-time applications [3]. Fast modern digital computers make such arguments less relevant. On the other hand, an algebraic closed-form representation of a dynamic model enables an explicit analysis of each effect, such as inertia, centripetal/Coriolis, gravity and friction, and a direct evaluation of their influence on the dynamic behavior. Direct insight into the model structure makes control design more

straightforward, as it facilitates compensation for each particular effect. For example, a closed-form model of gravity can be used in the compensation of gravitational loads. Having in mind advanced computation power and storage capabilities of modern digital computers, the online implementation of closed-form dynamic models for control purposes becomes possible. Unfortunately, the derivation of closed-form models in compact form, in particular inverse kinematic and dynamic models, is usually not easy, even if software for symbolic computation is used. The derivation demands a series of operations accompanied by permanent simplification of intermediate results. Hence, it is valuable to report any contribution in this area. When a model is derived, it is useful to establish its correctness. Comparing it with some recursive representation of the same kinematics or dynamics is straightforward with available software packages. Software routines specialized for robotic problems are presented in, e.g., [9] and [10].

### B. Estimation of Model Parameters

When a model is available, the next step is obtaining its parameters, so the model corresponds to the real system. Kinematic parameters, such as link lengths, twist angles and link offsets, are usually known with better accuracy than inertial ones: link masses, locations of their centers of mass, and link moments of inertia. The kinematic parameters are either directly provided by the robot manufacturer or can be achieved by direct measurements on the robot. Adjustment of these parameters can be done via kinematic calibration [5]. As for the inertial parameters, they are rarely provided by the manufacturer, but are rather reconstructed by the robot users. Friction modeling and estimation are also important issues, as friction may cause control problems, e.g., static errors or stick-slip, possibly leading to limit cycles.

There is an extensive literature on estimation of inertial and friction parameters [5],[8], [11]–[31]. Here we present an overview of some results. When estimating inertial parameters, for each robot link one should determine one mass, three Cartesian coordinates of the center of mass and six elements of the inertia tensor [3], [5]. In this general case, for a robot with  $n$  links, there exist  $n \times 10$  unknowns. In practice, instead of estimating each parameter, it is more common to identify algebraic combinations that constitute a so-called base parameters set (BPS). Elements of this set can be uniquely identified in experiments. There exists a representation of the dynamic model linear in the elements of the BPS [1], [5], [8], [11]–[18], [31]. The regression matrix depending on the robot trajectory, i.e., the motions, speeds, and accelerations, premultiplies the BPS in vector form to equate the control inputs. The total energy is also linear in the BPS [8], [11], [16]. The linearity property facilitates the estimation of the BPS.

1) *Friction Modeling and Estimation:* Friction is a complex interaction between the contact surfaces of the interacting objects, which can be represented with a number of models [19]–[30]. These models are used for theoretical analysis of friction phenomena and for control purposes. In this paper, the emphasis is on the latter one, i.e., model-based compensation of robot friction. Two friction regimes are observed: presliding

and sliding [19], [20]. Presliding occurs if the interacting objects are not moving relative to each other, while sliding arises after the relative motion is established. The level of friction prior to the sliding regime is called the static friction, or the stiction. It is determined by balancing the static forces acting on the interacting objects. Sophisticated friction models, e.g., the LuGre model [19]–[21], [23]–[25], characterize the presliding regime by stiffness and damping of dynamic interaction between the contact surfaces. At the beginning of the sliding regime, the friction force reduces as the speed is increasing, this is known as the Stribeck effect. Beyond this stage, the friction force increases as the speed is getting higher.

The basic friction model, covering just Coulomb and viscous effects, admits a linear parameterization, which enables simultaneous estimation of its parameters with the BPS elements [8], [12], [16]–[18]. Contrary to the basic one, more involved friction models are typically not linear in some parameters, and their parameters should be determined separately from the BPS. The three-sigmoidal-function model considered in [22] is an example of such a friction model. This model is used in Section IV.B. If a control designer adopts a model which is not linear in all parameters, then one has the following options: 1) to identify friction parameters separately from the BPS and use the fixed estimates for friction compensation [19], [20], [22]–[25], [29], [30]; 2) to estimate friction parameters online, simultaneously with using the model for friction compensation [21], [27], [28]; and 3) to give up of a structured friction model and adopt some nonmodel-based friction compensation strategy, including the direct sensing of friction using force sensors [28]. The first option is often used in robot control, and it will be demonstrated in Section IV.B.

2) *Estimating the Inertial Parameters:* Once a strategy for friction modeling, estimation, or measurement is decided, one may proceed with estimation of the BPS. For that purpose an identification experiment has to be designed. During the experiment, the robot performs specific motions, implemented using a decentralized control approach. This means use of decoupled proportional integral derivative (PID) controllers to generate control inputs. The data needed for the parameter estimation are the control inputs and motion coordinates, i.e., displacements, speeds and, if necessary, accelerations. These data are obtained by direct measurements and/or are reconstructed using filters or observers.

The reliability of the estimation depends on the trajectory executed by the robot during the identification experiments. The so-called excitation trajectory should be carefully designed, and this is done by optimizing some property of the information matrix [8], [11], [12], [14], [16]–[18]. This matrix is formed by vertically stacking the regression matrices that correspond to different points of the excitation trajectory. The condition number of the information matrix, its largest singular value, its Frobenius condition number, the determinant of the weighted product between the information matrix and its transpose, are some choices for the performance criteria to be optimized. No matter which performance criterion is adopted, the resulting optimization problem is most likely nonconvex, which means that the global optimal excitation trajectory cannot be obtained

easily. Different initial conditions may lead to different excitation trajectories, all corresponding to local minima of the optimization criterion. As argued in [11], “engineering judgment, patience, and good luck are required to find a good trajectory.” Here, we would like to review what researchers consider as “a good excitation trajectory,” and which requirements, in our opinion, it should satisfy.

Computing the excitation trajectory using calculus of variations is suggested in [11]. The optimization problem was to minimize the condition number of the Persistent Excitation matrix, created using the information matrix. The objective was to increase the immunity of estimation in the presence of measurement noise. The optimization algorithm generated a complete excitation trajectory, point by point. Such trajectory representation was referred to as “the general one,” which means that the space of trajectories to be searched is not restricted. This, in general, may contribute to an inefficient optimization process. The same problem is inherent to the method of generating excitation trajectories presented in [14]. Once again, the trajectory is computed point by point, narrowing the search space only by imposing constraints on permissible ranges of robot motions, speeds and accelerations. Furthermore, both approaches do not explicitly specify the frequency content of the computed trajectories. This is an additional drawback, as control of the frequency content is an important precaution for avoiding frequency components that may excite the robot flexibility. The intentional parameterization of an excitation trajectory is a way to impose the desired frequency content, and to narrow the search space for the purpose of faster optimization. For example, in [17] and [18] the excitation trajectories are postulated as finite Fourier series with predefined fundamental frequency and with coefficients to be determined by optimizing some performance criterion. The resulting trajectories are periodic, which enables continuous repetition of the identification experiment and averaging of measured data to improve signal-to-noise ratio. Additional merits are that, by design, one may enforce the desired frequency resolution and the frequency content of the trajectories.

The excitation trajectories are realized on the robotic systems using PID feedback controllers. The resulting control inputs and the motion coordinates are measured and recorded for estimation of the BPS elements. Several estimation algorithms, from the least-squares to maximum-likelihood methods, are investigated so far. The success of sophisticated algorithms strongly depends on an accurate knowledge of statistical properties of the signal noise and of other disturbances affecting the signals in use. Some algorithms were experimentally compared in [31]. The most involved estimation algorithm based on the maximum-likelihood method indeed showed the best performance, but the achieved improvements over the simpler algorithms do not seem so striking. An alternative for advanced estimation techniques is to improve the quality of the signals measured on the robotic system, by reducing the impact of disturbances [32]–[36]. A comparative study of several digital techniques for speed estimation from position measurements is given in [32]. The effectiveness of these techniques for estimation of acceleration was not argued, so their usefulness

in obtaining data of sufficient quality for the BPS estimation cannot be immediately anticipated. On the other hand, one may use Kalman filtering [33], as formulated in [34]–[36], to optimally reconstruct all motion coordinates including acceleration, in the presence of measurement noise and uncertainty in system dynamics. If the reconstructed motion coordinates are used, then even the simplest least-squares estimation of the BPS elements gives satisfactory results.

3) *Experimental Model Validation*: After the estimation is finished, experimental validation of the model has to be done. A rigorous two-step validation strategy was established in [5]. The objective of the first step is to test how accurately the model reproduces outputs of PID controllers. If this accuracy is satisfactory, one proceeds to the second validation step: verification of the model's utility for control purposes.

In a number of publications on robot modeling and identification, just the first step of the validation strategy is considered. For instance, in [17], the validation is performed along a trajectory interpolating randomly chosen points in the robot workspace. The interpolation takes care of constraints on joint motions, speeds, and accelerations. It is expected that qualitative agreement of torques rendered by the model and measured torques under PID control, along such a random trajectory, is a sufficient guarantee of model correctness. A similar qualitative validation can be found in [18] and [31]. In [18], validation is performed along a smooth trajectory defined in the joint space. Choice of a sine wave as the validation trajectory, as in [31], is probably the simplest validation one might consider, as it tests the model for just one harmonic component. Satisfactory results for a single harmonic do not necessarily imply the same for other frequency components.

In [5], experimental validation was carried out using a fifth-order polynomial trajectory, defined in joint space. The trajectory was chosen to ensure fast joint motions, requiring full authority of all drives. First, the considered dynamic model was validated qualitatively, i.e., by comparing its output with measured torques under proportional derivative (PD) control. Then, the model was implemented in two control algorithms—feedforward and computed-torque control—to generate control inputs in addition to the PD feedback. The latter test verified that the model-based control realizes smaller tracking errors, when compared with the errors achieved with the simple PD control.

In this paper, the experimental model validation is performed similarly as in [5], but along a trajectory with a more involved shape and by implementing the dynamic model only in the feedforward control algorithm. The effectiveness of the model in a computed-torque like control algorithm was experimentally verified in [37]–[39]. Our validation trajectory is a sequence of letters with a prescribed velocity profile, defined in task space. We consider handwriting, as a dynamic model should be validated along a trajectory sufficiently general to induce motions similar to those a robot is supposed to perform in practice. For example, industrial robots typically realize movements along concatenated straight-line and curved paths in their task spaces. Writing of letters is indeed a concatenation of straight-line and curved primitives. Additionally, the

handwriting may impose significant demands on the robot dynamics due to varying speed levels and discontinuous accelerations. The handwriting in robotics was presented in [40], [41]. Surveys of related research results are available in [42] and [43], also presenting the sequence of letters we use for model validation.

### C. Dynamics not Covered with a Model

A dynamic model is used in model-based control algorithms. It contributes to the performance of the applied control algorithms to the extent it matches the real robot dynamics. In practice, the model, especially a rigid-body one, may cover the real dynamics only within the low-frequency range, as the real dynamics encompass flexible effects at higher frequencies. These effects are caused by elasticity in joints and by distributed link flexibilities [44]. If one requires high performance, the influence of flexible modes cannot be disregarded. On the contrary, theoretical and experimental studies presented in [37]–[39] show that knowledge of the dynamics not covered by a dynamic model is essential for improved performance and robustness. Therefore, in this paper we make a step further from the conventional objective to model and identify just the rigid-body dynamics, signifying a need to also identify dynamics not covered by the rigid-body model.

## III. ROBOT MODELING

### A. Kinematics and Dynamics in Closed-Form

A wire frame kinematic model of a robotic arm representing the robot class considered in this paper is shown in Fig. 1. A minimal kinematic parameterization of the arm, according to the well-known Denavit–Hartenberg (DH) notation [1], [3], is established and presented in Table I. The DH parameters are: twist angles  $\alpha_i$ , link lengths  $a_i$ , joint displacements  $q_i$ , and link offsets  $d_i$ , where  $i = 1, \dots, n$ . Obviously, the arm has  $n = 3$  revolute degrees-of-freedom (d.o.f.s), and therefore we call it the RRR robotic arm.

The position and orientation of the  $i$ th coordinate frame with respect to the previous one ( $i - 1$ ) can be specified by the homogenous transformation matrix

$${}^{i-1}_i\mathbf{T}(\mathbf{q}) = \begin{bmatrix} {}^{i-1}_i\mathbf{O}(\mathbf{q}) & {}^{i-1}_i\mathbf{x}(\mathbf{q}) \\ \mathbf{0}_{1 \times 3} & 1 \end{bmatrix} \quad (1)$$

where  $\mathbf{q}$  is a vector of joint motions

$$\mathbf{q} = [q_1 \quad q_2 \quad q_3]^T \quad (2)$$

a skew-symmetric rotation matrix  ${}^{i-1}_i\mathbf{O} \in \mathbb{R}^{3 \times 3}$  defines the orientation of the  $i$ th frame with respect to frame  $i - 1$ , and the vector  ${}^{i-1}_i\mathbf{x} \in \mathbb{R}^{3 \times 1}$  contains the Cartesian coordinates of frame  $i$ , expressed in coordinate frame  $i - 1$ . Expressions for  ${}^{i-1}_i\mathbf{O}$  and  ${}^{i-1}_i\mathbf{x}$  can be found in any text-book on robotics (e.g., in [1] and [3]). The RRR robotic arm is an open kinematic chain, so its forward kinematics can be computed as a product of homogenous transformations between the circumjacent coordinate frames

$${}^0_3\mathbf{T}(\mathbf{q}) = {}^0_1\mathbf{T}(\mathbf{q}) {}^1_2\mathbf{T}(\mathbf{q}) {}^2_3\mathbf{T}(\mathbf{q}) = \begin{bmatrix} {}^0_3\mathbf{O}(\mathbf{q}) & {}^0_3\mathbf{x}(\mathbf{q}) \\ \mathbf{0}_{1 \times 3} & 1 \end{bmatrix}. \quad (3)$$

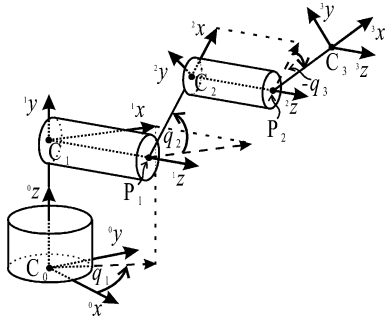


Fig. 1. Kinematic model of an RRR robotic arm.

TABLE I  
DH PARAMETERS OF AN RRR ROBOTIC ARM

$i$	$\alpha_i$	$a_i$	$q_i$	$d_i$
1	$\pi/2$	0	$q_1$	$C_0C_1$
2	0	$P_1C_2$	$q_2$	$C_1P_1$
3	0	$P_2C_3$	$q_3$	$C_2P_2$

Particular expressions for  ${}^0_3\mathbf{O}$  and  ${}^0_3\mathbf{x}$  are given by (A1) and (A2), in Appendix . A closed-form representation of the inverse kinematics (IK), formula (A3), is also given. This representation has at least three advantages: 1) it enables direct recognition of “irregular” robot configurations, such as kinematic singularities; 2) by specifying a sign in the expression for  $q_3$ , we may explicitly take control over the actual robot posture – the arm can reach each point in the Cartesian space either with the elbow up (–sign) or with the elbow-down (+sign); and 3) an analytic IK solution requires less computations as compared with any iterative numerical method. The last property will be verified by an example presented in the next section.

The rigid-body model of the robot dynamics can be derived using the Euler–Lagrange formulation [1]–[3], [8]. The standard form of the model is as follows:

$$\boldsymbol{\tau}(t) = \mathbf{D}(\mathbf{q}(t))\ddot{\mathbf{q}}(t) + \mathbf{c}(\mathbf{q}(t), \dot{\mathbf{q}}(t)) + \mathbf{h}(\mathbf{q}(t)) + \boldsymbol{\tau}^f(t) \quad (4)$$

where  $\mathbf{q}$  is defined by (2),  $\dot{\mathbf{q}}$  and  $\ddot{\mathbf{q}}$  are vectors of the joint speeds and accelerations, respectively,  $\mathbf{D}$  is the inertia matrix,  $\mathbf{c}$ ,  $\mathbf{g}$  and  $\boldsymbol{\tau}^f$  are the vectors of Coriolis/centrifugal, gravitational and friction effects, respectively, and  $\boldsymbol{\tau}$  is the vector of joint control inputs (torques). Elements of  $\mathbf{D}$ ,  $\mathbf{c}$  and  $\mathbf{h}$  can be determined from the homogenous transformation (1), using

$$\begin{aligned}
 d_{i,k} &= \sum_{j=\max(i,k)}^3 \text{Tr} \left[ \frac{\partial_j^0 \mathbf{T}}{\partial q_k} \mathbf{J}_j \left( \frac{\partial_j^0 \mathbf{T}}{\partial q_i} \right)^T \right] \\
 c_i &= \sum_{k=1}^3 \sum_{m=1}^3 c_{i,k,m} \dot{q}_k \dot{q}_m, \\
 c_{i,k,m} &= \sum_{j=\max(i,k,m)}^3 \text{Tr} \left[ \frac{\partial_j^{20} \mathbf{T}}{\partial q_k \partial q_m} \mathbf{J}_j \left( \frac{\partial_j^0 \mathbf{T}}{\partial q_i} \right)^T \right] \\
 h_i &= \sum_{j=i}^3 \left( -m_j \mathbf{g} \frac{\partial_j^0 \mathbf{T}}{\partial q_i} \mathbf{j}_j \right), \quad i, k, m = 1, 2, 3. \quad (5)
 \end{aligned}$$

Here,  $m_j$  is the mass of the  $j$ th link,  $\mathbf{j}_j \mathbf{r}$  contains the homogenous coordinates of the center of mass of link  $j$  expressed in the  $j$ th coordinate frame

$$\mathbf{j}_j \mathbf{r} = [x_j \quad y_j \quad z_j \quad 1]^T \quad (6)$$

$\mathbf{g}$  represents a gravity vector  $\mathbf{g} = [00 -g0]$  ( $g = 9.8062 \text{ m/s}^2$ ), while  $\mathbf{J}_j$  is the inertia tensor with elements

$$\begin{aligned}
 j_{j,11} &= \frac{-I_{xx,j} + I_{yy,j} + I_{zz,j}}{2}; \quad j_{j,22} = \frac{I_{xx,j} - I_{yy,j} + I_{zz,j}}{2} \\
 j_{j,33} &= \frac{I_{xx,j} + I_{yy,j} - I_{zz,j}}{2}; \quad j_{j,12} = j_{j,21} = I_{xy,j} \\
 j_{j,13} &= j_{j,31} = I_{xz,j}; \quad j_{j,23} = j_{j,32} = I_{yz,j} \\
 j_{j,14} &= j_{j,41} = m_j x_j; \quad j_{j,24} = j_{j,42} = m_j y_j \\
 j_{j,34} &= j_{j,43} = m_j z_j; \quad j_{j,44} = m_j. \quad (7)
 \end{aligned}$$

Here,  $I_{xx,j}$ ,  $I_{yy,j}$  and  $I_{zz,j}$  denote principal moments of inertia for the link  $j$ , and  $I_{xy,j}$ ,  $I_{yz,j}$  and  $I_{xz,j}$  are products of inertia of the same link.

The dynamic model (4), excluding friction, can be represented linearly in elements of the BPS. These elements are nonlinear combinations of the inertial parameters used in the equations above, and they represent the total set of parameters that can be uniquely estimated [11]–[18]. A linear parameterization of the rigid-body dynamic model (4) has the form

$$\boldsymbol{\tau}(t) = \mathbf{R}(\mathbf{q}(t), \dot{\mathbf{q}}(t), \ddot{\mathbf{q}}(t))\mathbf{p} + \boldsymbol{\tau}^f(t) \quad (8)$$

where  $\mathbf{R} \in \mathbb{R}^{3 \times 15}$  is the regression matrix and  $\mathbf{p} \in \mathbb{R}^{15 \times 1}$  is the vector of BPS elements.

Closed-form expressions of the elements of  $\mathbf{p}$  and  $\mathbf{R}$  are given by formulas (A4) and (A5) in the Appendix , respectively. These expressions reveal the complexity of the nonlinear robot dynamics, but also enable independent analysis of particular dynamical effects. With the elements of (A5) containing the gravitational constant  $g$  we may assemble gravitational terms, with the elements containing joint accelerations we may recover inertial terms, while the remaining elements define Coriolis/centrifugal terms. Equation (8) can be used for online compensation of the corresponding dynamic effects.

### B. Model Verification with a Writing Task

Writing tasks may require complex nonsmooth motions, whose execution can induce significant dynamic forces/torques. One representative writing task [42], [43] is presented in Fig. 2. It consists of writing a sequence of letters that can be described piecewise in closed-form, with the possibility of imposing an arbitrary velocity profile. Freedom in prescribing the velocity profile enables one to pose very demanding dynamic tasks, which is confirmed by the analysis carried out in [43]. The piecewise closed-form representation and the possibility of imposing the velocity can be exploited for a rigorous verification of robot kinematic and dynamic models.

The robot-tip should move along the planar path shown in Fig. 2(a) ( $y$  coordinate is fixed), with the continuous velocity profile

$$v(t) = \sqrt{\dot{x}^2(t) + \dot{z}^2(t)} \quad (9)$$

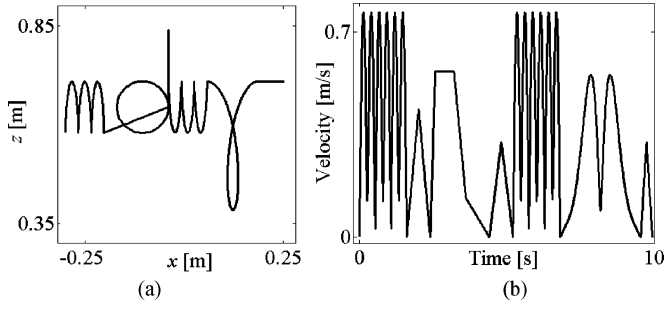


Fig. 2. Reference trajectory in the task space. (a) Tip path and (b) adopted tip-velocity profile.

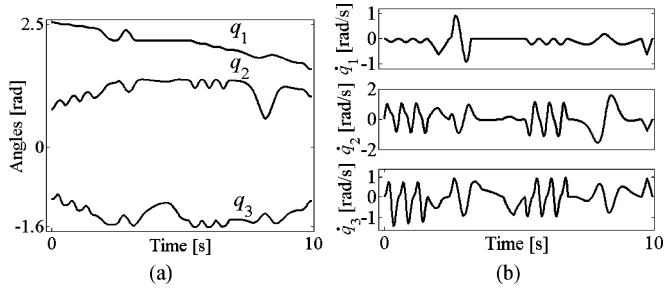


Fig. 3. Trajectory in joint space for the writing task. (a) Motions and (b) speeds.

presented in Fig. 2(b). The profile has fast and slow phases. Fig. 2 defines the reference tip trajectory. To determine the corresponding joint motions using (A3), the DH parameters were assigned to the values given in the next section. The joint motions and the related speeds are presented in Fig. 3, revealing the nonsmooth joint trajectory with significant speed levels. The joint motions were compared with the IK solution computed using an iterative method, implemented in the Robotics Toolbox for Matlab [10]. Guaranteed accuracy of the Robotics Toolbox solution is within  $10^{-10}$  rad. The differences between the closed-form and the Robotics Toolbox solutions were within the accuracy of the latter ones, verifying the correctness of (A3). The Robotics Toolbox was also used to establish the correctness of the closed-form rigid-body dynamic model (A4), (A5). All inertial parameters were assigned arbitrary nonzero values, positive for masses and principal moments of inertia, without sign constraint for products of inertia and coordinates of centers of masses. The model (A4), (A5) computed torques corresponding to the joint trajectory shown in Fig. 3. The torques were also calculated using a recursive routine implemented in the Robotics Toolbox. The differences between the two solutions were caused by round-off errors only, verifying the correctness of (A4) and (A5).

#### IV. CASE-STUDY

##### A. Experimental Setup

The robotic arm engaged for experimental identification is shown in Fig. 4. This experimental facility is used for research on modeling, identification and control of robots [6], [7], [37]–[39]. Its three rotational joints are actuated by gearless brushless DC direct-drive motors. The joints have infinite range of motions, since power and sensor signals are transferred via



Fig. 4. Experimental RRR robotic arm.

TABLE II  
DH PARAMETERS OF THE EXPERIMENTAL RRR ROBOTIC ARM

$i$	$\alpha_i$ [rad]	$a_i$ [m]	$q_i$	$d_i$ [m]
1	$\pi/2$	0	$q_1$	0.56
2	0	0.2	$q_2$	0.169
3	0	0.415	$q_3$	0.09

sliprings. Numerical values of the DH parameters are given in Table II. The actuators are Dynaserv DM-series servos with nominal torques of 60, 30, and 15 Nm, respectively. Each actuator has an integrated incremental optical encoder with a resolution of  $\sim 10^{-5}$  rad. These servos are driven by power amplifiers with built-in current controllers. Both encoders and amplifiers are connected to a PC-based control system. This system consists of a MultiQ I/O board from Quanser Consulting ( $8 \times 13$  bits ADC,  $8 \times 12$  bits DAC, 8 digital I/O, 6 encoder inputs, and three hardware timers), combined with the soft real-time system Wincon from Quanser Consulting. It facilitates online data acquisition and control directly from Matlab/Simulink. The rigid-body dynamics are dominant in the overall dynamic behavior of the RRR robot arm. Friction effects can be observed, too, together with several effects not covered by the rigid-body dynamics with friction, e.g., vibrations at the robot base and high-frequency resonances.

##### B. Friction Modeling and Estimation

A number of possibilities for friction modeling are available [19]–[30]. In this paper, we use the three-sigmoid-function friction model [22]

$$\tau_i^f = \sum_{k=1}^3 f_{i,k} \left( 1 - \frac{2}{e^{2w_{i,k}\dot{q}_i} + 1} \right) + b_i \dot{q}_i \quad (i = 1, 2, 3). \quad (10)$$

This model enables reconstruction of Stribeck, Coulomb, and viscous friction effects. It also admits a straightforward online

implementation. Since  $\tau_i^f$  is clearly zero at  $\dot{q}_i = 0$ , the model does not capture the static friction. Although there is ample evidence that compensation of static friction is important for high-performance robot control [19], [20], [28], our practical experience does not encourage its model-based compensation, but rather compensation via integral control.

As the parameters  $w_{i,k}$  appear nonlinearly, the friction model (10) cannot be parameterized linearly in all unknown parameters ( $f_{i,k}$ ,  $w_{i,k}$ , and  $b_i$ ). This prevents simultaneous estimation of the unknown parameters and the BPS elements, using, e.g., some time-efficient least-squares technique. Consequently, the friction parameters are estimated for each d.o.f. separately, using identification experiments in open-loop. In each experiment, the actuator for the considered d.o.f. is driven with a sufficiently exciting control input and the responding joint motion is measured. The remaining joints are kept locked by means of appropriate hardware or by feedback control. In the latter case, the feedback controllers must be tuned such that the motions in the remaining joints, possibly caused by couplings between the robot axes and by gravity, are prevented. The dynamics for joint  $i$  can be represented as

$$\ddot{q}_i = \frac{[\tau_i - \tau_i^f(f_{i,k}, w_{i,k}, b_i) - c_i \sin q_i]}{J_i} \quad (k = 1, 2, 3) \quad (11)$$

where  $J_i$  is the equivalent moment of inertia of the load on the shaft of the joint actuator and  $c_i$  is a coefficient of the gravity term. This term vanishes if the considered axis is parallel with the direction of gravity. The parameters  $J_i$  and  $c_i$  are usually not known exactly, so they need to be estimated together with the friction parameters. To estimate all unknowns, we use an extended Kalman filtering method elaborated in [22].

After repeating the estimation procedure for each d.o.f. of the RRR robotic arm, the estimates given in Table III were obtained. To assess how close the friction model matches the actual friction in the corresponding robot joint, we performed validation experiments for every d.o.f. For illustration, here we present the validation experiment for the third joint. In the experiment, the torque  $\tau_3(t)$  shown at the top in Fig. 5 was applied as the feed-forward control input. Gravity was compensated by closing the feedback loop via  $\hat{c}_3 \sin q_3$ , where  $\hat{c}_3$  is the estimate given in Table III. During the experiment, the responses  $q_3(t)$  and  $\dot{q}_3(t)$  to  $\tau_3(t)$  were measured. The identical input  $\tau_3(t)$  was applied to the model (11), taking into account the estimates from Table III. The simulated fractions of  $\tau_3(t)$  are presented in Fig. 5: friction torque  $\tilde{\tau}_3^f(t)$  computed via (10), gravitational load  $\hat{c}_3 \sin \tilde{q}_3(t)$ , and inertial load  $J_3 \ddot{\tilde{q}}_3(t)$ . The sign “ $\sim$ ” indicates simulated variables. The plots shown in Fig. 5 reveal significant contribution of friction to the joint dynamics. Similar contribution of friction can be observed in the other robot joints, too. To verify that the friction model (10) was correctly estimated, we compare the measured  $q_3(t)$  and  $\dot{q}_3(t)$  with the simulated  $\tilde{q}_3(t)$  and  $\tilde{\dot{q}}_3(t)$ . Two simulations were carried out: in the first one, the friction torque  $\tilde{\tau}_3^f(t)$  was disregarded; the second simulation took  $\tilde{\tau}_3^f(t)$  into account. The plots presented in Fig. 6(a), corresponding to the first simulation, show no match between the measured and the simulated motion coordinates. On the other hand,  $\tilde{q}_3(t)$  and  $\tilde{\dot{q}}_3(t)$  obtained in the second simulation, presented in Fig. 6(b),

TABLE III  
ESTIMATES OF FRICTION PARAMETERS AND INERTIAL PARAMETERS

Axis	Case 1	Case 2	Case 3	Case 4
$x$	1.0586183	0.8937624	0.8514829	0.9144705
$y$	1.7499008	1.6946019	1.4393078	1.7196776
$z$	4.5700627	3.7535460	3.3575332	3.7666039
Axis	Case 5	Case 6		
$x$	0.7174938	0.3269994		
$y$	0.4644522	0.2522228		
$z$	1.7217765	1.0738162		

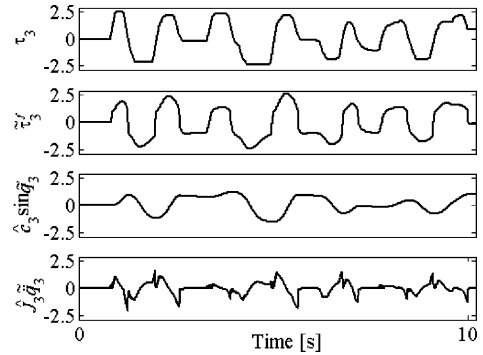


Fig. 5. Friction model validation for the third joint. Input torque, its friction, gravity, and inertial fractions.

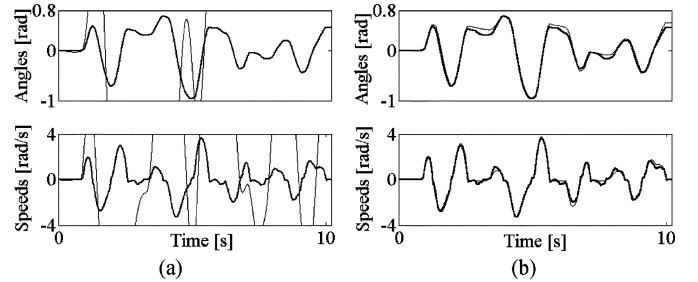


Fig. 6. Measured (thick) and simulated (thin) angular displacements and speeds in the third joint. (a) Friction torque disregarded in simulation. (b) Friction torque taken into account in simulation.

are in high agreement with the measurements, which validates the friction model with the estimated parameters. Similar results hold for the other joints, too.

### C. Estimation of the BPS

Here we work out the procedure to estimate the BPS  $\mathbf{p}$ . As already mentioned, formulas corresponding to all elements of  $\mathbf{p}$  are available in the Appendix (A4).

1) *Least-Squares Estimation Method*: Consider the rigid-body dynamics (8). Let us excite it with a control input  $\boldsymbol{\tau}(t)$  and collect the resulting  $\mathbf{q}(t)$ ,  $\dot{\mathbf{q}}(t)$  and  $\ddot{\mathbf{q}}(t)$ . Assume we have collected  $\zeta$  samples of each element of  $\boldsymbol{\tau}$ ,  $\mathbf{q}$ ,  $\dot{\mathbf{q}}$  and  $\ddot{\mathbf{q}}$ , corresponding to time instants  $t_1, t_2, \dots, t_\zeta$ . Since (8) holds for each  $t_k \in \{t_1, t_2, \dots, t_\zeta\}$ , we may form the following system of equations:

$$\Phi \cdot \mathbf{p} = \mathbf{y} \quad (12)$$



where

$$\Phi = \begin{bmatrix} \mathbf{R}(\mathbf{q}(t_1), \dot{\mathbf{q}}(t_1), \ddot{\mathbf{q}}(t_1)) \\ \mathbf{R}(\mathbf{q}(t_2), \dot{\mathbf{q}}(t_2), \ddot{\mathbf{q}}(t_2)) \\ \vdots \\ \mathbf{R}(\mathbf{q}(t_\zeta), \dot{\mathbf{q}}(t_\zeta), \ddot{\mathbf{q}}(t_\zeta)) \end{bmatrix} \quad (13)$$

$$\mathbf{y} = [(\boldsymbol{\tau}(t_1) - \boldsymbol{\tau}^f(t_1))^T, (\boldsymbol{\tau}(t_2) - \boldsymbol{\tau}^f(t_2))^T, \dots, (\boldsymbol{\tau}(t_\zeta) - \boldsymbol{\tau}^f(t_\zeta))^T]^T \quad (14)$$

assuming that the friction  $\boldsymbol{\tau}^f(t)$  is obtained by reconstruction or by measurements, as discussed in Section II.B.1. The input  $\boldsymbol{\tau}(t)$  is appropriate if it sufficiently excites the robot dynamics. With such excitation, the vector of identifiable parameters  $\mathbf{p}$  can be estimated in the least-squares (LS) sense, using some generalized inverse of the information matrix  $\Phi$

$$\hat{\mathbf{p}} = \Phi^* \mathbf{y} \quad (15)$$

where “\*” denotes a generalized matrix inverse [45].

To verify if the excitation used in the estimation of  $\mathbf{p}$  is appropriate, one may consider the condition number  $\aleph$  of  $\Phi$ . This is the ratio between maximal and minimal singular values of  $\Phi$ . As  $\aleph$  is closer to 1, more reliable estimation of  $\mathbf{p}$  is possible. In the literature, other criteria are also suggested and the representative choices have been listed in Section II.B.2. Here, we use the condition number only, as adopting another criterion does not influence the estimation procedure promoted. However, the LS estimation (15) gives relevant results only if the presence of disturbance effects in the collected motion coordinates  $\mathbf{q}$ ,  $\dot{\mathbf{q}}$  and  $\ddot{\mathbf{q}}$  is reduced to a minimum. High-frequency quantization noise is a commonly experienced disturbance. However, the use of carefully tuned Kalman observers for reconstruction of the motion coordinates can contribute to sufficient rejection of disturbances from the measurements. Online reconstruction is preferable, as it immediately provides us with the desired data. The reconstructed coordinates are then used in the LS estimation, which is the most time-efficient strategy. Use of more sophisticated estimation methods would probably lead to more accurate estimates of the BPS elements, however, on the cost of more effort, to identify the statistical properties of the signal noises. Our experimental experience shows that with the suggested simple but fast procedure, relevant estimates can be obtained.

2) *Reconstruction of the Motion Coordinates with a Kalman Observer*: Reconstruction of motion coordinates using a Kalman observer will be formulated in discrete-time, as signals are sampled. It is proven in [35] that at sufficiently high-sampling rates, usual in modern robotics, the discrete Kalman observer associated with the motion of a robot joint can be constructed assuming an all-integrator model for this motion. This model includes a correcting term  $\nu_i$ , representing the model uncertainty. It accounts for the difference between the adopted model and the real joint dynamics. The correcting term is a realization of the white process noise  $\xi_i$ , filtered through a linear, stable, all-pole transfer function. With the correcting term, to reconstruct speed, a second-order model or greater is required. If acceleration needs to be estimated, the model must be of order at least 3. Here, we adopt a third-order model for the case study, by assuming filtering  $\xi_i$  just through a

single integrator. In our experiments, this model is sufficient for estimating all the motion coordinates. Initially, we formulate the model in continuous time. If only the motion  $q_i$  is measured in joint  $i$ , the model for the Kalman observer design becomes

$$\ddot{q}_i = \ddot{q}_{r,i} + \nu_i; \quad \dot{\nu}_i = \xi_i; \quad \tilde{y}_i = q_i + \eta_i \quad (16)$$

where  $\ddot{q}_{r,i}$  is the desired joint acceleration and  $\eta_i$  is the measurement noise. In the design of the Kalman observer, we consider the deviation from the desired joint motion  $q_{r,i}$

$$e_i = q_i - q_{r,i} \quad (17)$$

and its time derivatives as the states to be reconstructed, rather than the motion coordinates itself. In such a way, the state reconstruction process is merely for the deviation from the expected, or modeled, trajectory [34]. Let  $T_s$  denotes the sampling time used for both data-acquisition and control. We may determine a discrete-time system having identical solutions with the model that arises after substituting (16) into (17)

$$\begin{aligned} \mathbf{x}_i(k+1) &= \mathbf{E}_i(T_s) \mathbf{x}_i(k) + \boldsymbol{\gamma}_i(T_s) \xi_i(k) \\ y_i(k) &= \mathbf{c}_i \mathbf{x}_i(k) + \eta_i(k), \end{aligned} \quad (18)$$

where

$$\mathbf{x}_i(k) = [e_i(k), \dot{e}_i(k), \nu_i(k)]^T \quad (19a)$$

$$\mathbf{E}_i = \begin{bmatrix} 1 & T_s & 0.5T_s^2 \\ 0 & 1 & T_s \\ 0 & 0 & 1 \end{bmatrix}, \quad \boldsymbol{\gamma}_i = \begin{bmatrix} \frac{T_s^3}{6} \\ 0.5T_s^2 \\ T_s \end{bmatrix} \quad (19b)$$

$$\mathbf{c}_i = [1 \quad 0 \quad 0]. \quad (19c)$$

The notation  $kT_s$  is rationalized with  $k$ . From (16), it follows that the output variable  $y_i$  is corrupted with noise  $\eta_i$ . A Kalman observer optimally reconstructs the states in the presence of model uncertainty and measurement noise

$$\hat{\mathbf{x}}_i(k+1) = \mathbf{E}_i(T_s) \bar{\mathbf{x}}_i(k), \quad \bar{\mathbf{x}}_i(k) = \hat{\mathbf{x}}_i(k) + \mathbf{k}_i [y_i(k) - \mathbf{c}_i \hat{\mathbf{x}}_i(k)] \quad (20)$$

where  $\bar{\mathbf{x}}_i$  denotes updated estimate of all states  $\mathbf{x}_i$ ,  $y_i$  is the difference between the measured and the reference joint motion (as in (18)), and  $\mathbf{k}_i$  is a  $n \times 1$  vector of constant gains. As the observer reconstructs deviations from the reference joint motions and speeds, together with the model uncertainty, the motion coordinates can be reconstructed as follows:

$$\bar{q}_i = q_{r,i} + \bar{e}_i, \quad \bar{\dot{q}}_i = \dot{q}_{r,i} + \bar{\dot{e}}_i, \quad \bar{\ddot{q}}_i = \ddot{q}_{r,i} + \bar{\nu}_i. \quad (21)$$

To compute the vector  $\mathbf{k}_i$ , one needs covariances of the measurement noise  $\eta_i$  and of the process noise  $\xi_i$ . Assuming white, zero mean quantization noise, uniformly distributed within a resolution increment  $\Delta\theta_m$  of the position sensor, the straightforward choice for the former variance is  $\Delta\theta_m^2/12$  (see [35] for details). There is a simple but effective rule to determine the latter variance, found in [34]. It is assigned to the square of the maximum jerk of the reference joint motion. In practice, these rules are used as initial guesses, while the final tuning is most effectively done online. Nevertheless, use of Bode plots from the measured  $e_i$  to the reconstructed  $\bar{e}_i$ , an illustrative example is presented in Fig. 7, could be instructive for filter tuning. The Bode plots reveal frequencies where harmonics will be amplified with the filter, as well as frequencies that

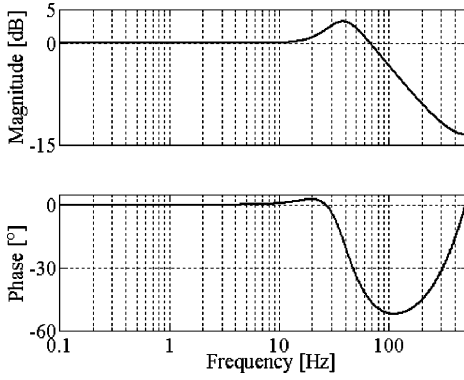


Fig. 7. Bode plots of the Kalman observer, from the measured  $e_i$  to the reconstructed  $\bar{e}_i$ .

the filter will attenuate. By analyzing the power spectrum of the error signal, a control engineer may locate spectral components due to noise and other disturbing effects, that need to be tackled via filtering. The gain vector  $\mathbf{k}_i$  can be retuned to reshape the Bode plot according to the needs.

3) *Design of Excitation Trajectories*: The design of excitation trajectories is done as in [17], [18]. The motion of each joint is postulated in the form of finite Fourier series to ensure cyclic movements during the identification experiment. The desired resolution of the frequency content  $\Delta f_i$  [Hz] defines the fundamental frequency of the Fourier series

$$q_i^{exc}(t) = q_{0,i} + \sum_{j=1}^{N_i} \frac{1}{j2\pi\Delta f_i} [a_{i,j} \sin(j2\pi\Delta f_i t) - b_{i,j} \cos(j2\pi\Delta f_i t)] \quad (i = 1, 2, 3). \quad (22)$$

The number of harmonics  $N_i$  defines the maximum frequency content of the excitation motions. Flexible effects of a direct-drive manipulator appear at higher frequencies [4], [5]. Therefore, rigid-body dynamics of these manipulators can be identified over a wide frequency range. We take advantage of this property to span frequencies of all trajectories that are admissible for the RRR robotic arm. Admissible are those trajectories that do not violate constraints on permissible speed and acceleration ranges, and do not excite flexible dynamics not contained in the adopted dynamic model. Technical constraints specify the following limits for speeds and accelerations of the RRR robot:  $|\dot{q}_1| \leq 2\pi$  rad/s,  $|\dot{q}_2| \leq 3\pi$  rad/s,  $|\dot{q}_3| \leq 3\pi$  rad/s, and  $|\ddot{q}_i| \leq 60$  rad/s<sup>2</sup> ( $i = 1, 2, 3$ ). An experimental study shows that joint motions within a bandwidth of 10 Hz do not excite flexibilities. Consequently, the excitation motions are postulated as in (22), with  $N_i = 100$  and  $\Delta f_i = 0.1$  Hz. This imposes frequency content up to 10 Hz and a cycle period of 10 s.

The coefficients  $q_{0,i}$ ,  $a_{i,j}$ , and  $b_{i,j}$  in (22) were found using an algorithm for constrained optimization which minimizes the condition number  $\aleph$  of the information matrix (13), under the constraints on permissible speeds and accelerations. The achieved minimum of  $\aleph$  was 3.1, inducing the excitation motions presented in Fig. 8. Here we should emphasize that we have no guarantee that we achieved the global minimum of  $\aleph$ , as the considered optimization problem is nonconvex. No

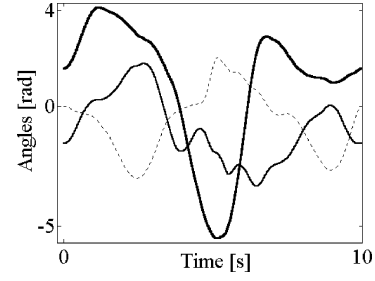


Fig. 8. Motions of excitation trajectories:  $q_1^{exc}$ —thick solid,  $q_2^{exc}$ —thin solid, and  $q_3^{exc}$ —dotted.

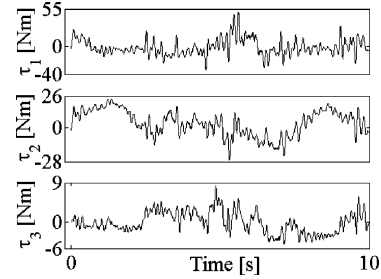


Fig. 9. Control inputs from the identification experiment.

matter if the excitation motions shown in Fig. 8 are globally optimal or suboptimal, they still can provide adequate estimates of the BPS elements, as we will show in the next two sections.

4) *Identification Experiment and Convergence of the BPS Elements*: The excitation trajectories were realized by applying a PD controller to each d.o.f. separately

$$\tau_i = -k_{p,i} \bar{e}_i - k_{d,i} \dot{\bar{e}}_i \quad (i = 1, 2, 3) \quad (23)$$

where  $\bar{e}_i$  is the online reconstructed difference between  $q_i^{exc}$  and the actual joint motion, and  $\dot{\bar{e}}_i$  is the online reconstructed time derivative of this difference. The gains in (23) were tuned using “trial and error,” to ensure reasonable tracking with a low level of noise in the control inputs  $\tau_i$  ( $i = 1, 2, 3$ ), as shown in Fig. 9. The sampling time was  $T_s = 1$  ms. As the parameters of the friction models (10) in all the joints have been estimated (Table III), these models were implemented online to compensate for the friction.

During the identification experiment, we acquired the generated inputs  $\tau_i(t)$  and the measurements  $\tilde{y}_i$  defined by (16) ( $i = 1, 2, 3$ ). We also online reconstructed and collected  $\tau_i^f(t)$ ,  $\bar{q}_i(t)$ ,  $\dot{\bar{q}}_i(t)$  and  $\ddot{\bar{q}}_i(t)$  ( $i = 1, 2, 3$ ). In Fig. 10(a), we present the differences between  $\tilde{y}_i$  and  $\bar{q}_i(t)$ . Since they are all below  $5 \times 10^{-4}$  rad, the accuracy in reconstructing the joint motions can be considered as good enough. The plots given in Fig. 10(b),(c) show the reconstructed  $\bar{q}_i(t)$  and  $\dot{\bar{q}}_i(t)$ , and indicate a low presence of noise. In Fig. 11, we present the online reconstructed friction torques  $\tau^f(t)$ . As demonstrated in Section IV.B, its reconstruction can be considered of sufficient quality to enable correction of the experimental  $\tau(t)$  and establish the relationship described with (12)–(14).

As all the data required by (15) is available, the LS estimation of the BPS elements can be carried out. To facilitate estimation, we take advantage of the symmetric mass distribution in the links 2 and 3, along the positive and negative directions of the axis <sup>2</sup> $y$ , respectively, <sup>3</sup> $y$  (see Fig. 1). These symmetries imply

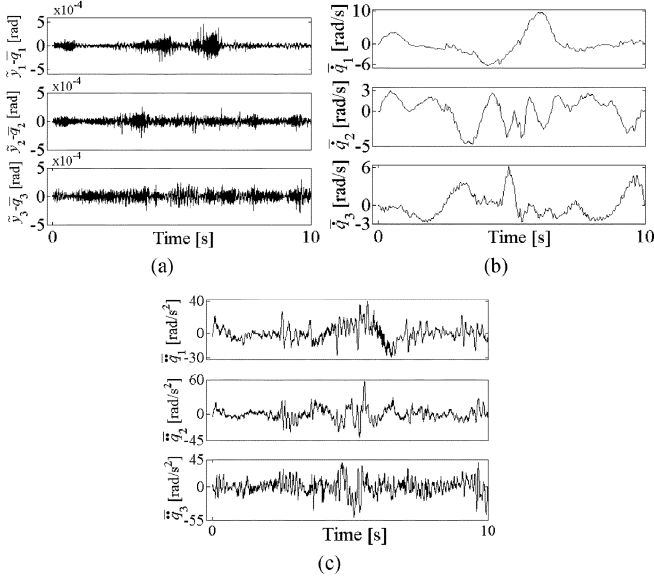


Fig. 10. Online reconstructing the motion coordinates. (a) Accuracy in reconstructing the joint motions  $-\hat{y}_i(t) - \bar{q}_i(t)$  ( $i = 1, 2, 3$ ). (b) Reconstructed joint speeds, and (c) the reconstructed joint accelerations.

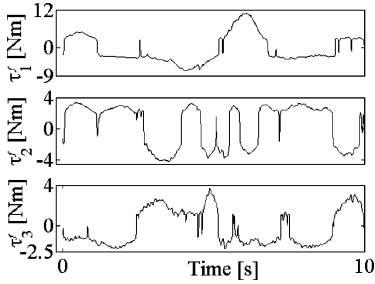


Fig. 11. Online reconstructed friction torques.

that the  $y_2$  coordinate of the link 2 center of mass and the  $y_3$  coordinate of the link 3 center of mass, are identically zero. By virtue of (A4), it follows that the elements  $p_4$  and  $p_{15}$  of the BPS are also identically zero. This reduces the dimensionality of the problem, as instead of all 15 parameters, only 13 elements of the BPS need estimation. As apparent from the plots shown in Fig. 12, the LS method results in the convergence of all 13 estimated elements of  $\hat{\mathbf{p}}$ . Their steady-state values are given in Table V.

**5) Experimental Model Validation:** To assess the quality of the estimates, a validation experiment with the writing task was performed. The objective was to check how good the estimated model reconstructs signals generated with the PD controllers (23) along the trajectory shown in Fig. 3. This trajectory corresponds to the writing task defined in Fig. 2. The setup used in the validation experiment is presented in Fig. 13. The realized joint motions, speeds and accelerations are online reconstructed with the Kalman observer (19)–(21). The computed motion coordinates are simultaneously fed into the estimated rigid-body model. The torques generated with the PD feedback controllers and the torques computed from the model are presented in Fig. 14. For each d.o.f., a close match between the experimental and the reconstructed signals is achieved. This implies a satisfactory estimation of the rigid-body dynamics.

Moreover, since the model reconstructs the control torques as the experiment is in progress, it follows that the dynamic model itself admits online implementation.

Another validation is model-based motion control of the robot. The rigid-body dynamic model (A4), (A5) with friction (10) was implemented as the feedforward controller to augment the basic PD feedback input [5]

$$\boldsymbol{\tau}(t) = \mathbf{R}(\mathbf{q}_r(t), \dot{\mathbf{q}}_r(t), \ddot{\mathbf{q}}_r(t))\mathbf{p} + \boldsymbol{\tau}^f(t) - \mathbf{K}_p(\bar{\mathbf{q}}(t) - \mathbf{q}_r(t)) - \mathbf{K}_d(\dot{\bar{\mathbf{q}}}_r(t) - \dot{\mathbf{q}}_r(t)) \quad (24)$$

where  $\mathbf{K}_p$  and  $\mathbf{K}_d$  are diagonal positive definite matrices of proportional and derivative gains, respectively. The PD feedback was based on online reconstructed joint motions and speeds [(19)–(21)]. The experimental servo setup corresponding to the model-based controller (24) is presented in Fig. 15. The controller was tested in the writing task defined by Figs. 2, 3. Six control cases were studied; the writing task was realized via: 1) PD feedback only; 2) PD feedback augmented with model-based friction compensation; 3) PD feedback augmented with model-based compensation of friction and inertial effects; 4) PD feedback augmented with model-based compensation of friction and centripetal/Coriolis effects; 5) PD feedback augmented with model-based compensation of friction and gravity effects; and 6) PD feedback augmented with the complete dynamic model with friction. Particular dynamic effects were extracted from the model (A4), (A5) as explained at the end of Section III.A. Identical PD gains were used for all case studied. These gains were weakly tuned, allowing a considerable discrepancy between the reference and executed motions, if the handwriting was executed using the PD feedback only. The reconstructed joint motions in all 6 case studies were processed via the forward kinematics model (A2) (in Appendix ), enabling visualization of the executed letters presented in Fig. 16. By inspection of the given plots, one notices that the first four case studies (figure on the left) achieve similar accuracy of handwriting. Thus, augmenting the PD feedback with the model-based friction compensation (case 2), as well as separate model-based compensation of inertial (case 3) and centripetal/Coriolis effects (case 4), do not improve motion performance. However, the PD feedback augmented with the model-based compensation of friction and gravity effects (case 5 in figure on the right) significantly improves accuracy of handwriting. This indicates that use of the model-based controller in addition to the basic PD feedback contributes to better motion performance. As apparent from the figure on the right hand side, the best accuracy was achieved with the PD feedback augmented with the complete dynamic model (case 6). In this case study, there is no visible discrepancy between the reference and executed sequences of letters. This demonstrates that the motion controller implementing the complete dynamic model achieves performance superior to controllers implementing just fractions of the complete model. Numerical verification of the given statements is presented in Table IV. This table shows standard deviations of the Cartesian errors between the reference and the reconstructed tip motions. The standard deviations corresponding to the last two cases are clearly smaller than the deviations achieved in the cases

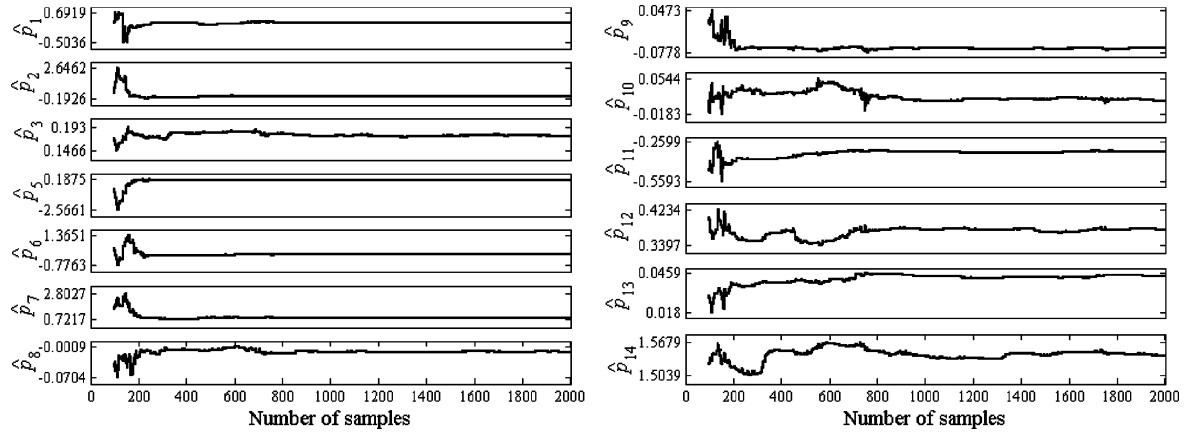


Fig. 12. Convergence of BPS estimates.

TABLE IV  
STANDARD DEVIATIONS OF THE TRACKING ERRORS IN THE TASK  
SPACE  $\times 10^{-3}$  [M]

Axis	Case 1	Case 2	Case 3	Case 4
$x$	1.0586183	0.8937624	0.8514829	0.9144705
$y$	1.7499008	1.6946019	1.4393078	1.7196776
$z$	4.5700627	3.7535460	1.7217765	3.7666039
Axis	Case 5	Case 6		
$x$	0.7174938	0.3269994		
$y$	0.4644522	0.2522228		
$z$	3.3575332	1.0738162		

TABLE V  
ESTIMATES OF BPS ELEMENTS

$\hat{p}_1$	$\hat{p}_2$	$\hat{p}_3$	$\hat{p}_5$	$\hat{p}_6$	$\hat{p}_7$	$\hat{p}_8$
0.2921	-0.0142	0.17306	0.07452	-0.0079	0.8180	-0.0116
$\hat{p}_9$	$\hat{p}_{10}$	$\hat{p}_{11}$	$\hat{p}_{12}$	$\hat{p}_{13}$	$\hat{p}_{14}$	
-0.0671	0.0062	-0.3434	0.3947	0.0440	1.5541	

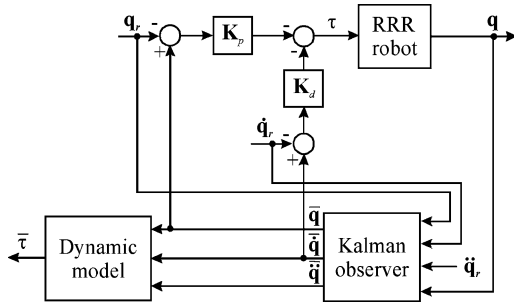


Fig. 13. Servo setup for experimental validation of the dynamic model.

1–4. Finally, we can claim that the estimated dynamic model successfully passed the experimental verification with the writing task.

#### D. Flexible Dynamics

In this part, we consider the robot motion control problem solved using the feedback linearization (computed-torque) control method [1], [5], [46]

$$\tau(t) = \mathbf{D}(\mathbf{q}(t))\mathbf{r}(t) + \mathbf{c}(\mathbf{q}(t), \dot{\mathbf{q}}(t)) + \mathbf{h}(\mathbf{q}(t)) + \tau^f(t). \quad (25)$$

Here,  $\mathbf{r}(t)$  represents a feedback control input, which should stabilize the robot motion and enforce the desired accuracy in realizing the reference joint trajectory  $\mathbf{q}_r(t)$ . The remaining variables are as defined in (4). When applied, the control (25) should decouple the robot dynamics. The problem of controlling the nonlinear-coupled system shifts to the problem of controlling the decoupled linear plants [37]–[39]

$$P_i(s) = \frac{q_i(s)}{r_i(s)} \quad (i = 1, \dots, n) \quad (26)$$

where  $r_i$  is the feedback control input applied at joint  $i$  and  $s$  is the complex variable. Ideally, the plant transfer function  $P_i$  would be modeled as a single mass, i.e., a double integrator. The related frequency response function should have a linear amplitude plot with a  $-2$  slope and constant phase at  $-180^\circ$ . This holds if a perfectly rigid-body robot dynamics is completely linearized by (25). In practice, this may not happen. Rather than a double integrator,  $P_i$  has a more involved frequency response, featuring resonance and anti-resonance frequencies. The location of these frequencies may vary as the robot changes its configuration. The importance of these flexible dynamics, not compensated with the dynamic model, on the quality of model-based motion control has been indicated already in [37]–[39]. Here we address their significance once again, to complete our discussion on robot modeling and identification.

The dynamic effects not covered with a rigid-body model influence the feasible levels of performance and robustness in robot control. Therefore, it is worthwhile spending additional effort on identifying these flexible dynamics. Here, we sketch an identification method capable of, at least, local identification of these dynamics as seen from the joint motion controller. To the best of our knowledge, the following method is not considered elsewhere in the literature on robot modeling and identification. The identification method makes use of the feedback linearization (25) with

$$\mathbf{r}(t) = -\mathbf{K}_p \mathbf{e}(t) - \mathbf{K}_d \dot{\mathbf{e}}(t) + \mathbf{v}(t) \quad (27)$$

where  $\mathbf{e} = \mathbf{q} - \mathbf{q}_r$  is already introduced,  $\mathbf{K}_p$  and  $\mathbf{K}_d$  are diagonal positive definite matrices of proportional and derivative gains, respectively, and  $\mathbf{v}$  stands for a persistent excitation. Here, for the speed error  $\dot{\mathbf{e}}$  one can use backward difference between two successive position measurements, divided with the time

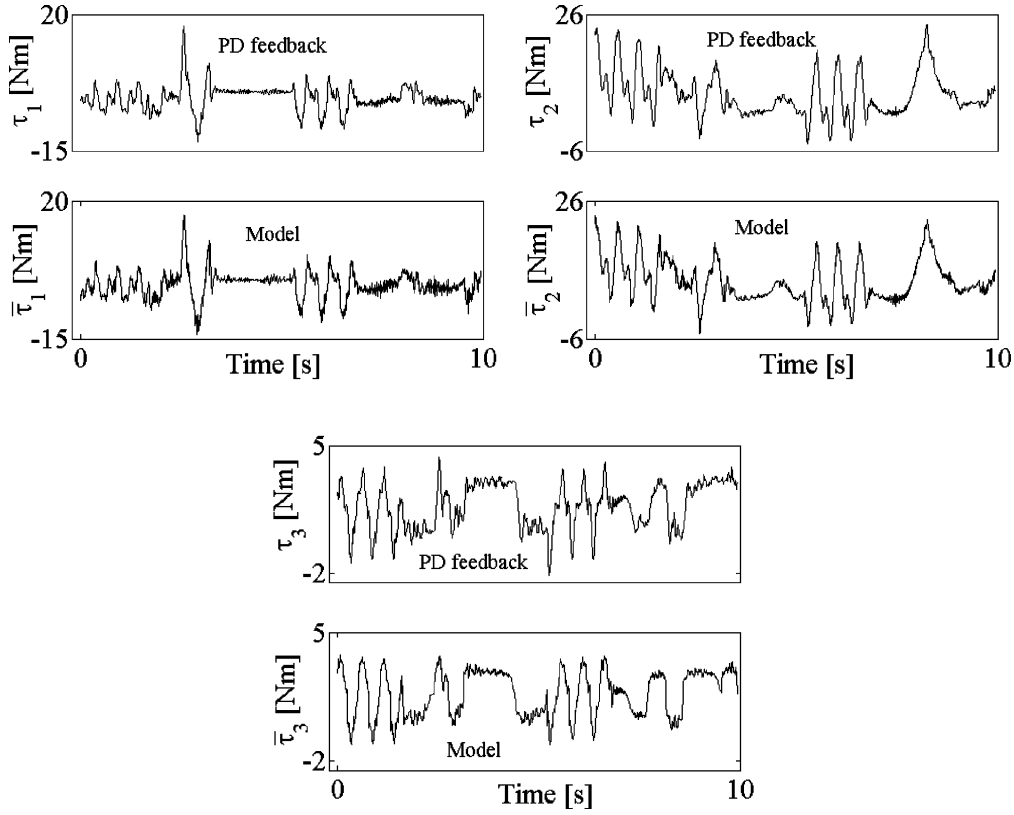


Fig. 14. Control torques produced with decentralized PD controllers and with the dynamic model in closed-form (measured in the experimental writing task).

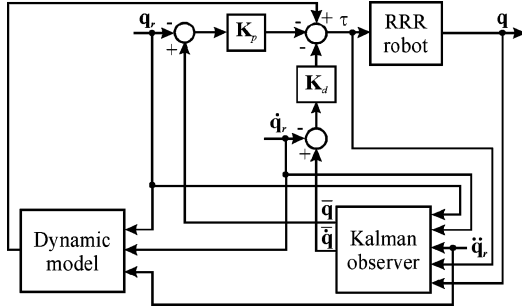


Fig. 15. Servo setup for experimental model-based control.

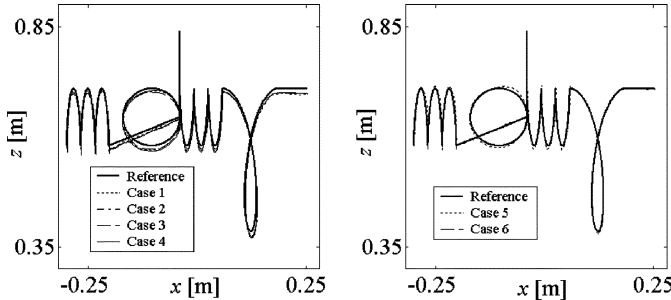


Fig. 16. Experimental results of model-based control.

between the measurements. Identification of flexible dynamics is performed for each d.o.f. separately. For example, if it is done for the  $i$ th d.o.f., the remaining joints are locked in fixed positions  $q_{r,j}$  ( $\dot{q}_{r,j} \equiv 0, j = 1, \dots, n, j \neq i$ ), while only the  $i$ th joint performs movements. As an example of such a movement, we propose a slow constant-speed motion of  $2\pi$  rad, with a change

in direction of movement after the full revolution is made. From our experience, making two full revolutions in mutually opposite directions is sufficient to acquire enough information for the purpose of identification. If joint motion is limited, a span of the joint range can be taken. The low-speed movement is needed to reduce the effect of friction, if it is not sufficiently well compensated with the friction model. The persistent excitation  $v$  could be, for example, a sequence of random numbers (noise). With a sampled-data implementation of (27), the persistent excitation cannot cover the complete frequency spectrum (white noise), but it will have a finite bandwidth determined by the sampling frequency. The response  $q_i(t)$  is measured for the given input  $r_i(t) = -k_{p,i}e_i(t) - k_{p,i}\dot{e}_i(t) + v_i(t)$ . The input and response data can be used to identify a frequency response function (FRF)  $P_i(j\omega) = q_i(j\omega)/r_i(j\omega)$  ( $\omega$  is angular frequency). However, as the identification is performed in closed loop, the obtained FRF might be unreliable. We characterize a FRF as unreliable if the coherence function [47]

$$\Gamma(\omega) = \Phi_{rq}^2(\omega)(\Phi_{qq}(\omega)\Phi_{rr}(\omega))^{-1} \quad (28)$$

is small. With  $\Phi_{rr}$  and  $\Phi_{qq}$ , we denote the autopower spectra of the control input  $r_i(t)$  and of the joint response  $q_i(t)$ , respectively, while  $\Phi_{rq}$  is the cross power spectrum between  $r_i(t)$  and  $q_i(t)$ . Provided all autopower spectra are nonzero,  $\Gamma$  is ideally 1 at all  $\omega$ , independently of  $q_i(t)$  and  $r_i(t)$ . The frequencies  $\omega$  where  $\Gamma$  is below 1 correspond to spectral components of  $q_i(t)$  that are corrupted by disturbances (e.g., noise). Disturbances degrade reliability of identification. From our experience, coherence below 0.7 indicates that the identified FRF is not reliable.

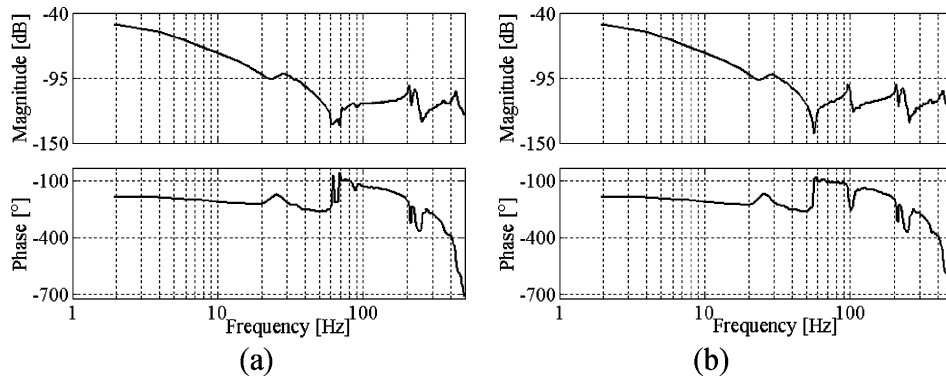


Fig. 17. Flexible dynamics for first d.o.f. corresponding to two fixed configurations of the remaining joints. (a)  $[q_2, q_3] = [0, \pi/2]$ . (b)  $[q_2, q_3] = [0, 0]$ .

In this case, one can resort to indirect identification, by measuring the frequency response from  $v_i(t)$  to  $r_i(t)$ . This is the FRF of the sensitivity function  $S_i (= 1/(1 + P_i C_i))$ ,  $C_i$  is the PD controller of the feedback loop in the  $i$ th joint. The indirect approach normally achieves coherence sufficient for reliable identification. With the identified sensitivity, for a known setting of the PD gains, one may restore  $P_i(j\omega)$  via

$$P_i(j\omega) = \frac{1 - S_i(j\omega)}{C_i(j\omega)S_i(j\omega)}. \quad (29)$$

The indirect identification was successfully tested on the RRR robotic arm; with such identification we normally achieve coherences close to 1. For illustration, in Fig. 17 we present FRFs measured in the first d.o.f., for two different configurations in the remaining joints. The first configuration is  $[q_2, q_3] = [0, \pi/2]$ , which, according to the schematic shown in Fig. 1, corresponds to a horizontal orientation of the second link and vertical upwards position of the last link. The second configuration corresponds to the stretched arm in the horizontal plane, i.e.,  $[q_2, q_3] = [0, 0]$ . The FRFs of both configurations reveal at low frequencies dynamics of the ideal plant, i.e., of a double integrator. However, around 28 Hz we may notice a modest resonance, caused by insufficient stiffness in mounting the robot base to the floor. Being highly damped and with a temporary phase lead (see the phase plots), it is not a problem for stability. However, it may cause vibrations of the robot mechanism and in turn degrade the robot performance. This is why it must not be disregarded if high-performance motion control is required. At higher frequencies (above 80 Hz), we may observe more profound resonances, whose location and damping factors depend on the robot posture. If amplified too much by feedback, these resonances may destabilise the closed-loop system. They can also contribute to amplification of vibrations and noise in the covered frequency ranges and consequently degrade the performance of motion control.

High performance model-based robot control, with sufficient robustness against parasitic dynamics and disturbances, is possible only if all notable peculiarities of the robot are recognized and taken into account during the control design. This certainly increases the time needed for robot identification and controller synthesis. However, the benefit is a robotic system of improved quality, without modifications of the system mechanics. Our experimental experiences [37]–[39] with model-based robot control confirm the given statement.

## V. CONCLUSION

This paper deals with the problems of modeling and identification for high-performance model-based control of a robot. To illustrate all the steps required to obtain the appropriate models, a robot class with three spatial rotational degrees of freedom is adopted as case study. For this class of robots, models of kinematics and rigid-body dynamics are derived in closed-form, and are presented in full detail. To stress the impact of nonlinear dynamic couplings, a direct-drive actuation of the robot joints is assumed. The correctness of the models is established in simulation. A straightforward but efficient estimation of parameters of the rigid-body dynamic model that includes friction effects is suggested. The estimation procedure is an effective compromise between the requirements from the available theory on robot identification and common knowledge of a control engineer. Guidelines for design of a persistently exciting identification trajectory are given. The estimation is simplified, as the need for identification of statistical properties of signal noises is avoided. All required motion coordinates, usually corrupted with disturbance effects (e.g., quantization noise), are reconstructed via a Kalman observer. As it filters out the disturbances, an efficient least-squares algorithm becomes a reliable solution for parameter estimation. The effectiveness of the procedure is experimentally demonstrated on a direct-drive robot. A writing task is suggested for rigorous validation of the quality of the obtained models. The rigid-body dynamic model with friction satisfactorily covers the experimental results. Its appropriateness for implementation in model-based control laws is also justified. However, it is also indicated that the rigid-body dynamic model is still not sufficient for a perfect match to the real robot dynamics, as in practice the dynamics may contain flexible effects not covered by this model. A procedure to identify these flexible dynamics is proposed. With these additional dynamics available, more advanced feedback control designs become possible. The results of the use of these models for model-based feedback design are promising and will be published separately.

## APPENDIX

### A. Kinematic Models in Closed-Form

Here we detail the forward kinematics model (3). To simplify notation, in the following we avoid the use of “ $\cdot$ ” and assume

that all coordinates of the tip are referred to the base coordinate frame “0.” The elements of the orientation matrix  $\mathbf{O}(\mathbf{q})$  are as follows:

$$\begin{aligned} o_{1,1} &= \cos q_1 \cos(q_2 + q_3), \quad o_{1,2} = -\cos q_1 \sin(q_2 + q_3) \\ o_{1,3} &= \sin q_1, \quad o_{2,1} = \sin q_1 \cos(q_2 + q_3) \\ o_{2,2} &= -\sin q_1 \sin(q_2 + q_3), \quad o_{2,3} = -\cos q_1 \\ o_{3,1} &= \sin(q_2 + q_3), \quad o_{3,2} = \cos(q_2 + q_3), \quad o_{3,3} = 0. \end{aligned} \quad (\text{A1})$$

The Cartesian coordinates  $x$ ,  $y$ , and  $z$  of the tip  ${}^0\mathbf{x}(\mathbf{q})$  are

$$\begin{aligned} x &= \cos q_1 (a_3 \cos(q_2 + q_3) + a_2 \cos q_2) + (d_2 + d_3) \sin q_1 \\ y &= \sin q_1 (a_3 \cos(q_2 + q_3) + a_2 \cos q_2) - (d_2 + d_3) \cos q_1 \\ z &= a_3 \sin(q_2 + q_3) + a_2 \sin q_2 + d_1. \end{aligned} \quad (\text{A2})$$

The inverse kinematics mapping is also computed in closed-form, by solving the (A2) for  $q_1$ ,  $q_2$  and  $q_3$

$$\begin{aligned} q_1 &= \text{asin} \frac{x(d_2 + d_3) + y\sqrt{x^2 + y^2 - (d_2 + d_3)^2}}{x^2 + y^2} \\ q_3 &= \text{atan} \frac{\pm \sqrt{1 - \frac{(p_{wh}^2 + p_{wv}^2 - a_2^2 - a_3^2)^2}{(2a_2 a_3)^2}}}{\frac{(p_{wh}^2 + p_{wv}^2 - a_2^2 - a_3^2)}{(2a_2 a_3)}} \\ q_2 &= \text{atan} \frac{(a_2 + a_3 \cos q_3)p_{wv} - a_3 \sin q_3 p_{wh}}{(a_2 + a_3 \cos q_3)p_{wh} + a_3 \sin q_3 p_{wv}} \\ p_{wh} &= \sqrt{[x - (d_2 + d_3) \sin q_1]^2 + [y + (d_2 + d_3) \cos q_1]^2} \\ p_{wv} &= z - d_1. \end{aligned} \quad (\text{A3})$$

### B. Dynamic Model in Closed-Form

A representation of the rigid-body dynamic model (8), linear in the BPS, is derived in closed-form

$$\begin{aligned} p_1 &= a_2^2 m_3 + a_2 m_2 (a_2 + 2x_2) - I_{xx,2} + I_{yy,2} \\ p_2 &= -2(a_2 m_2 y_2 + I_{xy,2}), \quad p_3 = m_3 (a_3 + x_3), \quad p_4 = m_3 y_3 \\ p_5 &= a_3 m_3 (a_3 + 2x_3) - I_{xx,3} + I_{yy,3} \\ p_6 &= 2(a_3 m_3 y_3 + I_{xy,3}) \\ p_7 &= 2d_2 m_2 z_2 + d_2^2 m_2 + 2(d_2 + d_3) m_3 z_3 \\ &\quad + (d_2 + d_3)^2 m_3 + I_{yy,1} + I_{xx,2} + I_{xx,3} \\ p_8 &= -(d_2 + d_3) m_3 y_3 - I_{yz,2} \\ p_9 &= -a_3 m_3 (z_3 + d_2 + d_3) - (d_2 + d_3) m_3 x_3 - I_{xz,3} \\ p_{10} &= -d_2 m_2 y_2 - I_{yz,2} \\ p_{11} &= -a_2 (m_3 (z_3 + d_2 + d_3) + m_2 (d_2 + z_2)) \\ &\quad - d_2 m_2 x_2 - I_{xz,2} \\ p_{12} &= (a_2^2 + a_3^2 + 2a_3 x_3) m_3 + a_2 m_2 (a_2 + 2x_2) \\ &\quad + I_{zz,2} + I_{zz,3} \\ p_{13} &= a_3 m_3 (a_3 + 2x_3) + I_{zz,3}, \quad p_{14} = m_2 (x_2 + a_2) + m_3 a_2 \\ p_{15} &= m_2 y_2. \end{aligned} \quad (\text{A4})$$

$$\begin{aligned} r_{1,1} &= \ddot{q}_1 \cos^2 q_2 - \dot{q}_1 \dot{q}_2 \sin(2q_2) \\ r_{1,2} &= 0.5 \ddot{q}_1 \sin(2q_2) + \dot{q}_1 \dot{q}_2 \cos(2q_2) \end{aligned}$$

$$\begin{aligned} r_{1,3} &= 2a_2[(\ddot{q}_1 \cos(q_2 + q_3) - \dot{q}_1 \dot{q}_3 \sin(q_2 + q_3)) \cos q_2 \\ &\quad - \dot{q}_1 \dot{q}_2 \sin(2q_2 + q_3)] \\ r_{1,4} &= -2a_2[(\ddot{q}_1 \sin(q_2 + q_3) + \dot{q}_1 \dot{q}_3 \cos(q_2 + q_3)) \cos q_2 \\ &\quad + \dot{q}_1 \dot{q}_2 \cos(2q_2 + q_3)], \\ r_{1,5} &= \ddot{q}_1 \cos^2(q_2 + q_3) - \dot{q}_1 (\dot{q}_2 + \dot{q}_3) \sin(2q_2 + 2q_3) \\ r_{1,6} &= -0.5 \ddot{q}_1 \sin(2q_2 + 2q_3) - \dot{q}_1 (\dot{q}_2 + \dot{q}_3) \cos(2q_2 + 2q_3) \\ r_{1,7} &= \ddot{q}_1, \\ r_{1,8} &= (\ddot{q}_2 + \ddot{q}_3) \cos(q_2 + q_3) - (\dot{q}_2 + \dot{q}_3)^2 \sin(q_2 + q_3) \\ r_{1,9} &= (\ddot{q}_2 + \ddot{q}_3) \sin(q_2 + q_3) + (\dot{q}_2 + \dot{q}_3)^2 \cos(q_2 + q_3) \\ r_{1,10} &= -\dot{q}_2^2 \sin q_2 + \ddot{q}_2 \cos q_2, \quad r_{1,11} = \dot{q}_2^2 \cos q_2 + \ddot{q}_2 \sin q_2 \\ r_{2,1} &= 0.5 \dot{q}_1^2 \sin(2q_2), \quad r_{2,2} = -0.5 \dot{q}_1^2 \cos(2q_2) \\ r_{2,3} &= 2a_2[(\ddot{q}_2 + 0.5 \ddot{q}_3) \cos q_3 - (0.5 \dot{q}_3^2 + \dot{q}_2 \dot{q}_3) \sin q_3 \\ &\quad + 0.5 \dot{q}_1^2 \sin(2q_2 + q_3)] + g \cdot \cos(q_2 + q_3), \\ r_{2,4} &= 2a_2[-(\ddot{q}_2 + 0.5 \ddot{q}_3) \sin q_3 - (0.5 \dot{q}_3^2 + \dot{q}_2 \dot{q}_3) \cos q_3 \\ &\quad + 0.5 \dot{q}_1^2 \cos(2q_2 + q_3)] - g \cdot \sin(q_2 + q_3) \\ r_{2,5} &= 0.5 \dot{q}_1^2 \sin(2q_2 + 2q_3), \quad r_{2,6} = 0.5 \dot{q}_1^2 \cos(2q_2 + 2q_3) \\ r_{2,8} &= \ddot{q}_1 \cos(q_2 + q_3), \quad r_{2,9} = \ddot{q}_1 \sin(q_2 + q_3) \\ r_{2,10} &= \ddot{q}_1 \cos q_2, \quad r_{2,11} = \ddot{q}_1 \sin q_2, \quad r_{2,12} = \ddot{q}_2, \quad r_{2,13} = \ddot{q}_3 \\ r_{2,14} &= g \cdot \cos q_2, \quad r_{2,15} = -g \cdot \sin q_2 \\ r_{3,3} &= a_2[(0.5 \dot{q}_1^2 + \dot{q}_2^2) \sin q_3 + \cos q_3 \ddot{q}_2 \\ &\quad + 0.5 \dot{q}_1^2 \sin(2q_2 + q_3)] + g \cdot \cos(q_2 + q_3) \\ r_{3,4} &= a_2[(0.5 \dot{q}_1^2 + \dot{q}_2^2) \cos q_3 - \ddot{q}_2 \sin q_3 \\ &\quad + 0.5 \dot{q}_1^2 \cos(2q_2 + q_3)] - g \cdot \sin(q_2 + q_3) \\ r_{3,5} &= 0.5 \dot{q}_1^2 \sin(2q_2 + 2q_3), \quad r_{3,6} = 0.5 \dot{q}_1^2 \cos(2q_2 + 2q_3) \\ r_{3,8} &= \ddot{q}_1 \cos(q_2 + q_3), \quad r_{3,9} = \ddot{q}_1 \sin(q_2 + q_3) \\ r_{3,13} &= \ddot{q}_2 + \ddot{q}_3 \\ r_{1,12} &= r_{1,13} = r_{1,14} = r_{1,15} = r_{2,7} = r_{3,1} = r_{3,2} = 0 \\ r_{3,7} &= r_{3,10} = r_{3,11} = r_{3,12} = r_{3,14} = r_{3,15} = 0. \end{aligned} \quad (\text{A5})$$

### C. Friction Parameters and BPS Elements

Estimates of all parameters of the model (10), obtained using an EKF, are presented in Table III.

Estimates of all elements of the BPS are presented in Table V.

### REFERENCES

- [1] L. Sciacivco and B. Siciliano, *Modeling and Control of Robot Manipulators*. New York: McGraw-Hill, 1996.
- [2] M. Vukobratović and V. Potkonjak, *Dynamics of Manipulation Robots: Theory and Application*. Berlin, Germany: Springer-Verlag, 1982.
- [3] K. S. Fu, R. C. Gonzales, and C. S. G. Lee, *Robotics: Control, Sensing, Vision, and Intelligence*. New York: McGraw-Hill, 1987.
- [4] H. Asada and K. Youcef-Toumi, *Direct-Drive Robots: Theory and Practice*. Cambridge, MA: MIT Press, 1987.
- [5] C. H. An, C. G. Atkeson, and J. M. Hollerbach, *Model-Based Control of a Robot Manipulator*. Cambridge, MA: MIT Press, 1988.
- [6] B. van Beek and B. de Jager, “RRR-robot design: Basic outlines, servo sizing, and control,” in *Proc. IEEE Int. Conf. Control Applications*, Hartford, CT, 1997, pp. 36–41.
- [7] —, “An experimental facility for nonlinear robot control,” in *Proc. IEEE Int. Conf. Control Applications*, Kohala Coast, HI, 1999, pp. 668–673.
- [8] K. Kozłowski, *Modeling and Identification in Robotics*. New York: Springer-Verlag, 1998.

- [9] J. Nethery and M. W. Spong, "Robotica: A mathematica package for robot analysis," *IEEE Robot. Automat. Mag.*, vol. 1, pp. 13–20, Mar. 1994.
- [10] P. I. Corke, "A robotics toolbox for MATLAB," *IEEE Robot. Automat. Mag.*, vol. 3, pp. 24–32, Mar. 1996.
- [11] B. Armstrong, "On finding exciting trajectories for identification experiments involving systems with nonlinear dynamics," *Int. J. Robot. Res.*, vol. 8, no. 6, pp. 28–48, 1989.
- [12] M. Gautier and W. Khalil, "On the identification of the inertial parameters of robots," in *Proc. IEEE Conf. Dec. Control*, Austin, TX, 1988, pp. 2264–2269.
- [13] H. Mayeda, K. Yoshida, and K. Osuka, "Base parameters of manipulator dynamic models," *IEEE Trans. Robot. Automat.*, vol. 6, pp. 312–321, June 1990.
- [14] M. Gautier and W. Khalil, "Exciting trajectories for the identification of base inertial parameters of robots," *Int. J. Robot. Res.*, vol. 11, no. 4, pp. 362–375, 1992.
- [15] S. K. Lin, "Minimal linear combinations of the inertial parameters of a manipulator," *IEEE Trans. Robot. Automat.*, vol. 11, no. 3, pp. 360–373, 1995.
- [16] K. R. Kozlowski and P. Dutkiewicz, "Experimental identification of robot and load dynamics," in *Proc. 13th Triennial IFAC World Congr.*, San Francisco, CA, 1996, pp. 397–402.
- [17] J. Swevers, C. Ganseman, D. B. Tukel, J. de Schutter, and H. van Brussel, "Optimal robot excitation and identification," *IEEE Trans. Robot. Automat.*, vol. 13, pp. 730–740, Oct. 1997.
- [18] G. Calafiore, M. Indri, and B. Bona, "Robot dynamic calibration: Optimal excitation trajectories and experimental parameter estimation," *J. Robot. Syst.*, vol. 18, no. 2, pp. 55–68, 2001.
- [19] B. Armstrong-Hélouvy, P. Dupont, and C. C. de Wit, "A survey of models, analysis tools and compensation methods for the control of machines with friction," *Automatica*, vol. 30, no. 7, pp. 1083–1138, 1994.
- [20] H. Olsson, K. J. Åström, C. Canudas de Wit, M. Gäfvert, and P. Lischinsky, "Friction models and friction compensation," *Eur. J. Control*, vol. 4, no. 3, pp. 176–195, 1998.
- [21] C. Canudas de Wit and P. Lischinsky, "Adaptive friction compensation with partially known dynamic friction model," *Int. J. Adapt. Control Sig. Process.*, vol. 11, no. 1, pp. 65–80, 1997.
- [22] R. H. A. Hensen, G. Z. Angelis, M. J. G. van de Molengraft, A. G. de Jager, and J. J. Kok, "Grey-box modeling of friction: An experimental case study," *Eur. J. Control*, vol. 6, no. 3, pp. 258–267, 2000.
- [23] J. Swevers, F. Al-Bender, C. G. Ganseman, and T. Prajogo, "An integrated friction model structure with improved presliding behavior for accurate friction compensation," *IEEE Trans. Automat. Contr.*, vol. 45, pp. 675–686, Apr. 2000.
- [24] V. Lampaert, J. Swevers, and F. Al-Bender, "Modification of the Leuven integrated friction model structure," *IEEE Trans. Automat. Contr.*, vol. 47, pp. 683–687, Apr. 2002.
- [25] D. Kostić, R. Hensen, B. de Jager, and M. Steinbuch, "Modeling and Identification of an RRR-robot," in *Proc. IEEE Conf. Decision Control*, Orlando, FL, 2001, pp. 1144–1149.
- [26] —, "Closed-form kinematic and dynamic models of an industrial-like RRR robot," in *Proc. IEEE Conf. Robotics Automation*, Washington, DC, 2002, pp. 1309–1314.
- [27] B. de Jager, "Improving the tracking performance of mechanical systems by adaptive extended friction compensation," *Control Eng. Pract.*, vol. 1, no. 6, pp. 1009–1018, 1993.
- [28] L. R. Ray, A. Ramasubramanian, and J. Townsend, "Adaptive friction compensation using extended Kalman-Bucy filter friction compensation," *Control Eng. Pract.*, vol. 9, no. 2, pp. 169–179, 2001.
- [29] R. H. A. Hensen, M. J. G. van de Molengraft, and M. Steinbuch, "Frequency domain identification of dynamic friction model parameters," *IEEE Trans. Contr. Syst. Technol.*, vol. 10, pp. 191–196, Mar. 2001.
- [30] S. J. Kim and I. J. Ha, "A frequency-domain approach to identification of mechanical systems with friction," *IEEE Trans. Automat. Contr.*, vol. 46, pp. 888–893, Nov. 2001.
- [31] M. M. Olsen and H. G. Petersen, "A new method for estimating parameters of a dynamic robot model," *IEEE Trans. Robot. Automat.*, vol. 17, pp. 95–100, Feb. 2001.
- [32] R. H. Brown, S. C. Schneider, and M. G. Mulligan, "Analysis of algorithms for velocity estimation from discrete position versus time data," *IEEE Trans. Ind. Electron.*, vol. 39, pp. 11–19, Feb. 1992.
- [33] A. Gelb, *Applied Optimal Estimation*. Cambridge, MA: MIT Press, 1996.
- [34] P. R. Bélanger, "Estimation of angular velocity and acceleration from shaft encoder measurements," in *Proc. IEEE Int. Conf. Robotics Automation*, Nice, France, 1992, pp. 585–592.
- [35] P. R. Bélanger, P. Dobrovolny, A. Helmy, and X. Zhang, "Estimation of angular velocity and acceleration from shaft-encoder measurements," *Int. J. Rob. Res.*, vol. 17, no. 11, pp. 1225–1233, 1998.
- [36] H. Berghuis and H. Nijmeijer, "Robust control of robots via linear estimated state feedback," *IEEE Trans. Automat. Contr.*, vol. 39, pp. 2159–2162, Oct. 1994.
- [37] D. Kostić, B. de Jager, and M. Steinbuch, "Experimentally supported control design for a direct drive robot," in *Proc. IEEE Int. Conf. Control Applications*, Glasgow, U.K., 2002, pp. 186–191.
- [38] —, "Control design for robust performance of a direct-drive robot," in *IEEE Int. Conf. Control Applications*, Istanbul, Turkey, 2003, pp. 1448–1453.
- [39] B.H.M. Bukkems, D. Kostić, A.G. de Jager, and M. Steinbuch, "Frequency domain iterative learning control for direct drive robots," in *Eur. Control Conf.*, Cambridge, U.K., 2003.
- [40] J. M. Hollerbach, "Understanding manipulator control by synthesizing human handwriting," in *Artificial Intelligence: An MIT Perspective*. Cambridge, MA: MIT Press, 1979, vol. 1, pp. 311–332.
- [41] —, "An oscillation theory of handwriting," *Biol. Cybern.*, vol. 39, pp. 139–156, 1981.
- [42] V. Potkonjak, M. Popović, M. Lazarević, and J. Sinanović, "Redundancy problem in writing: From human to anthropomorphic robot arm," *IEEE Trans. Syst., Man, Cybern. B*, vol. 28, pp. 790–805, Dec. 1998.
- [43] V. Potkonjak, S. Tzafestas, D. Kostić, G. Djordjević, and M. Rašić, "Illustrating man-machine motion analogy in robotics – The handwriting problem," *IEEE Rob. Automat. Mag.*, vol. 10, pp. 35–46, Mar. 2003.
- [44] A. De Luca, "Feedforward/feedback laws for the control of flexible robots," in *Proc. IEEE Int. Conf. Robotics Automation*, San Francisco, CA, 2000, pp. 233–240.
- [45] G. H. Golub and C. F. van Loan, *Matrix Computations*. Baltimore, MD: The John Hopkins Univ. Press, 1996.
- [46] H. Nijmeijer and A. van der Schaft, *Nonlinear Dynamical Control Systems*. Berlin, Germany: Springer-Verlag, 1991.
- [47] L. Ljung, *System Identification: Theory for the User*. Englewood Cliffs, NJ: Prentice-Hall, 1987.



**Dragan Kostić** (S'98) received the B.Sc. and M.Sc. degrees in automatic control and robotics from the Faculty of Electronic Engineering, University of Niš, Serbia, in 1994 and 2000, respectively, and the Ph.D. degree with the Dynamics and Control Technology Group, Department of Mechanical Engineering, Technische Universiteit Eindhoven, The Netherlands, in 2004.

As a Research and Teaching Assistant with the Group for Automatic Control, Faculty of Electronic Engineering, University of Niš (1996–1999), he was investigating problems of biomechanics and ergonomics. His current research interests include dynamic modeling, system identification, robust model-based control of nonlinear mechanical systems, in particular robots, and data-based control of motion systems.

**Bram de Jager** received the M.Sc. degree in mechanical engineering from Delft University of Technology, Delft, The Netherlands, and the Ph.D. degree from the Technische Universiteit Eindhoven, The Netherlands.

He was with Delft University of Technology and Stork Boilers BV, Hengelo, The Netherlands. Currently, he is with the Technische Universiteit Eindhoven. His research interests include robust control of (nonlinear) mechanical systems, integrated control and structural design, control of fluidic systems, control structure design, application of symbolic computation in nonlinear control.





**Maarten Steinbuch** (S'83–M'89–SM'02) received the M.Sc. degree (*cum laude*) in mechanical engineering and the Ph.D. degree in modeling and control of wind energy conversion systems from Delft University of Technology, Delft, The Netherlands, in 1984 and 1989, respectively.

He is currently a Full Professor in Department of Mechanical Engineering, Technische Universiteit Eindhoven, Eindhoven, The Netherlands. From 1984 to 1987, he was a Research Assistant at Delft University of Technology and KEMA (Power

Industry Research Institute), Arnhem, The Netherlands. From 1987 to 1998, he was with Philips Research Laboratories, Eindhoven, as a Member of the Scientific Staff, working on modeling and control of mechatronic applications. From 1998 to 1999, he was Manager of the Dynamics and Control group at Philips Center for Manufacturing Technology. His research interests are modeling and control of motion systems.

Dr. Steinbuch was an Associate editor of the IEEE TRANSACTIONS ON CONTROL SYSTEMS TECHNOLOGY from 1993 to 1997, of *IFAC Control Engineering Practice* from 1994 to 1996, and of IEEE CONTROL SYSTEMS MAGAZINE from 1999 to 2002. He is currently Editor-at-Large of the *European Journal of Control*. In 2003, he received the Best-Teacher 2002/2003 award from the Department of Mechanical Engineering, Technische Universiteit Eindhoven.



**Ron Hensen** received the M.Sc. degree in mechanical engineering and the Ph.D. degree with the title "Controlled mechanical systems with friction," both from Technische Universiteit Eindhoven, The Netherlands.

He is currently a Scientific Researcher at DAF Trucks N.V., Eindhoven, The Netherlands. His main focus is on braking and stability control of commercial vehicles. From 2002 to 2004, he was a Member of the Mechatronical Engineering Department of Integrated Dynamics Engineering (IDE), Weert, The

Netherlands, and working on the control of high-performance semiconductor robots and vibration isolation systems.